Physical and biological forcing of mesoscale variability in the carbonate system of the Ross Sea (Antarctica) during summer 2014

Paola Rivaro [a],*, Carmela Ianni [a], Leonardo Langone [b], Carlo Ori [b], Giuseppe Aulicino [c], Yuri Cotroneo [c], Maria Saggiomo [d], Olga Mangoni [e]

[a] Department of Chemistry and Industrial Chemistry, University of Genoa, via Dodecaneso 31, 16146 Genova, Italy
[b] National Research Council of Italy, Institute of Marine Sciences, Via Gobetti 101, 40129 Bologna, Italy
[c] Department of Science and Technology, Parthenope University, Centro Direzionale, Isola C4 IT-80143 Napoli, Italy
[d] Stazione Zoologica Anton Dohrn, Villa Comunale 1, 80121 Napoli, Italy
[e] Department of Biology, University of Napoli Federico II, via Mezzocannone 8, 80134 Napoli, Italy

ABSTRACT

Water samples (0–200 m) were collected in a coastal area of the Ross Sea in January 2014 to evaluate the physical and biological forcing on the carbonate system at the mesoscale (distance between stations of 5–10 km). Remote sensing supported the determination of the sampling strategy and helped positioning each sampling station. Total alkalinity, pH, dissolved oxygen, phytoplankton pigments and composition were investigated in combination with measurements of temperature, salinity and current speed. Total inorganic carbon, sea water CO_2 partial pressure and the saturation state (Ω) for calcite and aragonite were calculated from the measured total alkalinity and pH. In addition, continuous measurements of atmospheric CO_2 concentration were completed. LADCP measurements revealed the presence of a significant change in current speed and direction that corresponded to a clearly defined front characterized by gradients in both temperature and salinity. Phytoplankton biomass was relatively high at all stations and the highest values of chlorophyll-a were found between 20 to 50 m, with the dominant taxonomic group being haptophyceae. The carbonate system properties in surface waters exhibited mesoscale variability with a horizontal length scale of about 10 km. Sea-ice melt, through the input of low salinity water, results in a dilution of the total alkalinity and inorganic carbon, but our observations suggest that phytoplankton activity was the major forcing of the distribution of the carbonate system variables. Higher CO_3^-, Ω and pH in the surface layer were found where the highest values of chlorophyll-a were observed. The calculated $\Delta p CO_2$ pattern follows both MODIS data and in situ chlorophyll-a measurements, and the estimated CO_2 fluxes ranged from -0.5 ± 0.4 to -31.0 ± 6.4 mmol m^{-2} d^{-1}. The large range observed in the fluxes is due to both the spatial variability of sea water $p CO_2$ and to the episodic winds experienced.

© 2015 Elsevier B.V. All rights reserved.

1. Introduction

The Ross Sea is one of the most productive regions of the Southern Ocean, exhibiting high levels of biomass and primary production, and high flows of biogenic material accumulations on the continental shelf (Armand et al., 2005; Arrigo et al., 2008; Catalano et al., 2010; Saggiomo et al., 1998, 2002; Smith and Comiso, 2008; Smith and Gordon, 1997). Ocean color imagery shows that the phytoplankton blooms are spatially extremely variable in the Ross Sea, even when the surface waters are ice free (Reddy and Arrigo, 2006). In fact, the Ross Sea is characterized by a complex array of ecosystems, each contributing differently to the primary production processes at the basin scale (Peloquin and Smith, 2007). Many differences are known to exist between coastal/offshore waters and thickness of the upper mixed layer (UML) relative to the composition of phytoplankton, as well as in the origin and development of the blooms and transfer of C within the food web (Mangoni et al., 2004; Saggiomo et al., 2002; Smith et al., 2010).

Phytoplankton blooms occur during the austral spring and summer, especially in the waters next to marginal ice zones, within polynyas, and on continental shelves (Garrity et al, 2005; Mangoni et al., 2009a; Moore and Abbott, 2000; Reddy and Arrigo, 2006; Saggiomo et al., 2002; Sullivan et al, 1993). Furthermore, a restricted number of functional groups contribute to this productivity and dominance varies at different temporal and spatial scales (Mangoni et al., 2004; Smith et al., 2010). The two dominant functional groups in the Ross Sea, diatoms and haptophytes (mainly *Phaeocystis antarctica*) have different temporal and spatial distributions, with *P. antarctica* generally dominating in spring in water columns with deeper vertical mixing and diatoms dominating in more stratified summer conditions (Arrigo et al., 1999; Di Tullio et al., 2003; Goffart et al., 2000; Smith et al., 2014). The

* Corresponding author. Tel.: +39 010 3536172; fax +39 010 3536190.
E-mail address: rivaro@chimica.unige.it (P. Rivaro).

phytoplankton blooms are dominated by diatoms such as *Fragilariopsis* and *Pseudonitzschia* species (Armand et al., 2005; Leventer and Dunbar, 1996; Saggiomo et al., 2000). Diatoms account for about 75% of the primary production in the Southern Ocean, regulate the cycle of silicon and support most food webs in the Antarctic (Knox, 1994; Mangoni et al., 2004; Smith and Asper, 2001; Tréguer et al., 1995). However, Smith et al. (2011a) estimated the diatom production in the southern Ross Sea to an average of ca. 40% per year. *P. antarctica* occurs in colonial form, but also as solitary cells, and the two forms have distinct ecological roles. It is known that the colonial haptophytes *P. antarctica* typically bloom in austral spring and reach high abundance (Smith et al., 2014; Tremblay and Smith, 2007), and disappear rapidly from the water column after reaching seasonal maximum (Smith et al., 2011a). The colonies of *P. antarctica* are not preferred by most of herbivorous micro- and meso-zooplankton and are removed through sinking and aggregation (Verity and Smetacek, 1996; Caron et al., 2000; DiTullio et al., 2000; Haberman et al., 2003). Therefore, the relative abundance of diatoms or *P. antarctica* can play an important role in shaping its food web and can influence the export of carbon to depth (Di Tullio et al., 2000; Schoemann et al., 2005; Smith et al., 2014; Sweeney et al., 2000).

The Ross Sea is an important region in the global carbon cycle and air–sea carbon dioxide fluxes (Arrigo et al., 1999, 2008; Catalano et al., 2010; Iudicone et al., 2011; Mangoni et al., 2009b). A modeling study has shown that the Ross Sea shelf waters are a strong trap for CO_2 due to high productivity, intense winds, high ventilation rates and extensive winter sea ice cover (Arrigo et al., 2008). The same study also confirmed that the Ross Sea has an important role in the anthropogenic CO_2 (CO_{2antr}) sequestration (Caldeira and Duffy, 2000; Sabine et al., 2004; Sandrini et al., 2007), as Antarctic Bottom Water (AABW) production occurs in the area (Orsi and Wiederwohl, 2009).

Throughout the ocean, mesoscale processes (on spatial scales of 10–100 km and temporal ranges from hours to days) have first-order impacts on phytoplankton physiochemical controls, and are critical in determining growth patterns and distribution; however, the mechanisms responsible for this variability are not yet well understood (Kaufman et al., 2014). The circulation of the Antarctic Surface Water (AASW) in the Ross Sea is affected by the presence of small-scale structures such as eddies, fronts and filaments. These mesoscale structures can penetrate deep below the ocean surface layer and hence influence the intensity of the bloom by supplying nutrients and trace elements, such as iron, to surface waters (McGillicuddy et al., 2007; Sweeney et al., 2003).

Little is known about the effects of mesoscale structures on the carbonate system and the air–sea CO_2 fluxes and carbon export (Chen et al., 2008; González-Dávila et al., 2003, 2006; Omand et al., 2015). The main features of the carbonate system in the Ross Sea have been described, showing both a large spatial and seasonal variability (Manno et al., 2007; Rivaro et al., 2014; Sandrini, et al., 2007). Therefore, the investigation of the mesoscale physical and biological forcing that determine the carbonate system variability is of particular importance to predict future modifications associated with climate change in the Ross Sea.

The primary objective of the RoME (Ross Sea Mesoscale Experiment) was to document the mesoscale distribution and spatial–temporal variability of biogeochemical properties of the upper 200 m layers in the Ross Sea with a horizontal resolution of 5–10 km. To this purpose, RoME used a combination of remote sensing and high resolution ship measurements during a cruise in the austral summer 2013–14, as part of the Italian National Program of Research in Antarctica (PNRA – Programma Nazionale di Ricerca in Antartide). Remote sensing supported both the determination of our sampling strategy and the placement of in situ stations. In this paper we investigate the role played by physical and biological processes on the mesoscale variability of the carbonate system and on the local air–sea CO_2 flux in a coastal area.

2. Materials and methods

2.1. Sampling strategy and water sampling

In situ data were collected aboard the R/V Italica, as part of the PNRA–RoME. Twelve stations consisting of 5–7 depths (2–200 m) were sampled from 26 to 28 January 2014 within the mesoscale RoME 2 survey (Fig. 1A). Surface and intermediate layers were sampled in all stations, while sampling to the bottom layer was completed at stations 33, 36, 39, 43 and 45. The position of the stations was chosen based on MODIS (Moderate Resolution Imaging Spectroradiometer) Aqua and Terra satellites level-2 products relative to the previous 12/24 h. Sea surface temperature (SST) and chlorophyll-a concentration (Chl-a) maps at 1 km resolution (Fig. 1B and C) were generated, analyzed and transmitted to the ship to allow sampling of both high and low chlorophyll regions. Sampling depths were chosen according to the fluorescence profiles. Station 35 was reoccupied after 2 days (station 45). Hydrological casts and water sampling were carried out using a SBE 9/11 Plus CTD, with dual temperature and conductivity sensors, coupled with a SBE 32 plastic coated carousel sampler, on which 24 12-L Niskin bottles were mounted. A couple of Lowered Acoustic Doppler Current Profiler (LADCP) was deployed together with the CTD to obtain current fields every 10 m from the surface to the maximum depth sampled. Tidal component has been successively removed according to Erofeeva et al. (2005).

2.2. Analytical procedures

2.2.1. Dissolved oxygen, phytoplankton pigments, taxonomic composition and maximum quantum yield of PSII.

Dissolved oxygen (O_2) was measured by the Winkler method using automated micro-titrations (Grasshoff, 1983) with a potentiometric detection of the end point using a Methohm 719 titroprocessor. The measurement precision was ± 0.5 mg L^{-1}.

Samples (4 L) for the determination of phytoplankton were collected at five or six depths from 0–100 m. Subsamples were analyzed for total biomass, size-fractionated Chl-a and composition determined by spectrofluorometric and HPLC analyses, respectively, and by microscopic analysis. Fractionation of phytoplankton was performed by serial filtration (see Mangoni et al., 2004). The filters for spectrofluorometric analyses of Chl-a and phaeopigments were stored at -80 °C and analyzed with a Varian Eclipse spectrofluorometer (Holm-Hansen et al., 1965). The instrument was checked daily with a Chl-a standard solution (from *Anacystis nidulans*; Sigma). For HPLC pigment analysis, 2–3 L of seawater were filtered under low light through Whatman GFF filters (47 mm), quickly frozen in liquid nitrogen, and stored at -80 °C until analysis. Pigment separation was performed by Hewlett Packard HPLC (mod. 1100) according to Vidussi el al. (1996). Calibrations used 20 pigments provided by the International Agency for [14]C Determination, VKI Water Quality Institute. Calculation of the relative abundance of various phytoplankton groups from the pigment concentrations was completed using CHEMTAX (Mackey et al., 1996). Samples for phytoplankton identification were collected at four different depths according to florescence profile and preserved with formaldehyde (4% final concentration). Cell counts were performed with an inverted light microscope (Zeiss Axiophot) according to the Utermöhl method (Utermöhl, 1958). At the same four depths, electron transport rate (ETR) vs. irradiance curves were performed with a Phyto-PAM fluorometer (Walz GmbH, Effeltrich, Germany). The maximum quantum yield (Fv/Fm) of photochemical energy conversion in PSII was determined (Schreiber et al., 1994, 1995).

2.2.2. A_T and pH measurements

Water samples for total alkalinity (A_T) and pH analyses were collected in 500 mL borosilicate glass bottles using standard procedures (DOE, 2007). The samples were poisoned in the container with saturated

$HgCl_2$ to stop biological activity. Samples were then stored in dark, cold (+4 °C) conditions. A_T and pH were measured using the methods described in Rivaro et al. (2010). pH was expressed on the pH total scale (i.e. [H^+] as moles per kilogram of seawater, pH_T), which was determined using a potentiometric method that employed a combination glass/reference electrode with an NTC temperature sensor. The Tris(hydroxymethyl)aminomethane (TRIS) buffer used to standardize the pH electrode was prepared according to standard methods (DOE, 2007). The salinity of the TRIS buffer was 35. Both the TRIS buffer and the seawater samples were brought to the same temperature (25 ± 0.1 °C) using a thermostatic water bath before the measurements were completed. The pH_T values at 25 °C were then recalculated at in situ temperature and pressure conditions (pH in situ). The accuracy and precision of A_T measurements were evaluated using the CRM batch 123 provided by A. G. Dickson (Scripps Institution of Oceanography). The precision for A_T measures was ± 4.0 μmol kg^{-1} and the recovery was 99.8%. The precision of the pH measurement was ± 0.007 units and it was evaluated by repeated analysis of the A_T certified material.

2.3. Auxiliary carbonate system parameters calculation

The CO_2SYS program (CO_2-Sys, Pierrot et al., 2006) was used to calculate the total inorganic carbon (C_T), the sea water CO_2 partial pressure (pCO_{2SW}), the saturation state for calcite (Ω_{Ca}) and aragonite (Ω_{Ar}) from the measured A_T and pH. Equilibrium constants of CO_2 (K_1 and K_2) of Millero (2007) and total hydrogen ion scale (mol kg_{SW}^{-1}) for pH were used for the calculation. The estimated probable errors for the calculated parameters of the carbon system, using pH and A_T as input measurements, are ± 3.8 μmol kg^{-1} and ± 2.1 μatm, for C_T and pCO_2, respectively.

2.4. Atmospheric CO_2 measurements and sea–air CO_2 fluxes calculation.

Continuous measurements of atmospheric CO_2 concentrations (pCO_{2atm}) were conducted throughout RoME 2 by a Siemens Ultramat 5E analyzer (Ori et al., 1996). The measurement system is based on the comparison between signals from two infrared absorbing cells, one filled with a flux of synthetic air with constant CO_2 concentrations (~ 380 μatm) and the other filled with the air sample. The air sample was carefully dried by a cold trap (t < − 40 °C). The instrument was calibrated using the WMO-X85 scale with working standards of 385 and 447 μatm determined at the Monte Cimone Observatory (Sestola, Italy). CO_2 concentrations were acquired at 0.5 Hz frequency and processed to remove spikes due to the possible contamination from the ship during the CTD stations. The data were then filtered to consider only data with winds blowing from –90°/+ 90° with respect to the air inlet at the ship's bow. For CO_2 flux calculations, pCO_{2atm} concentration for each station was obtained as average of at least 1200 values, then the data was corrected to 100% humidity at in situ sea surface temperature (SST) and salinity (SSS).
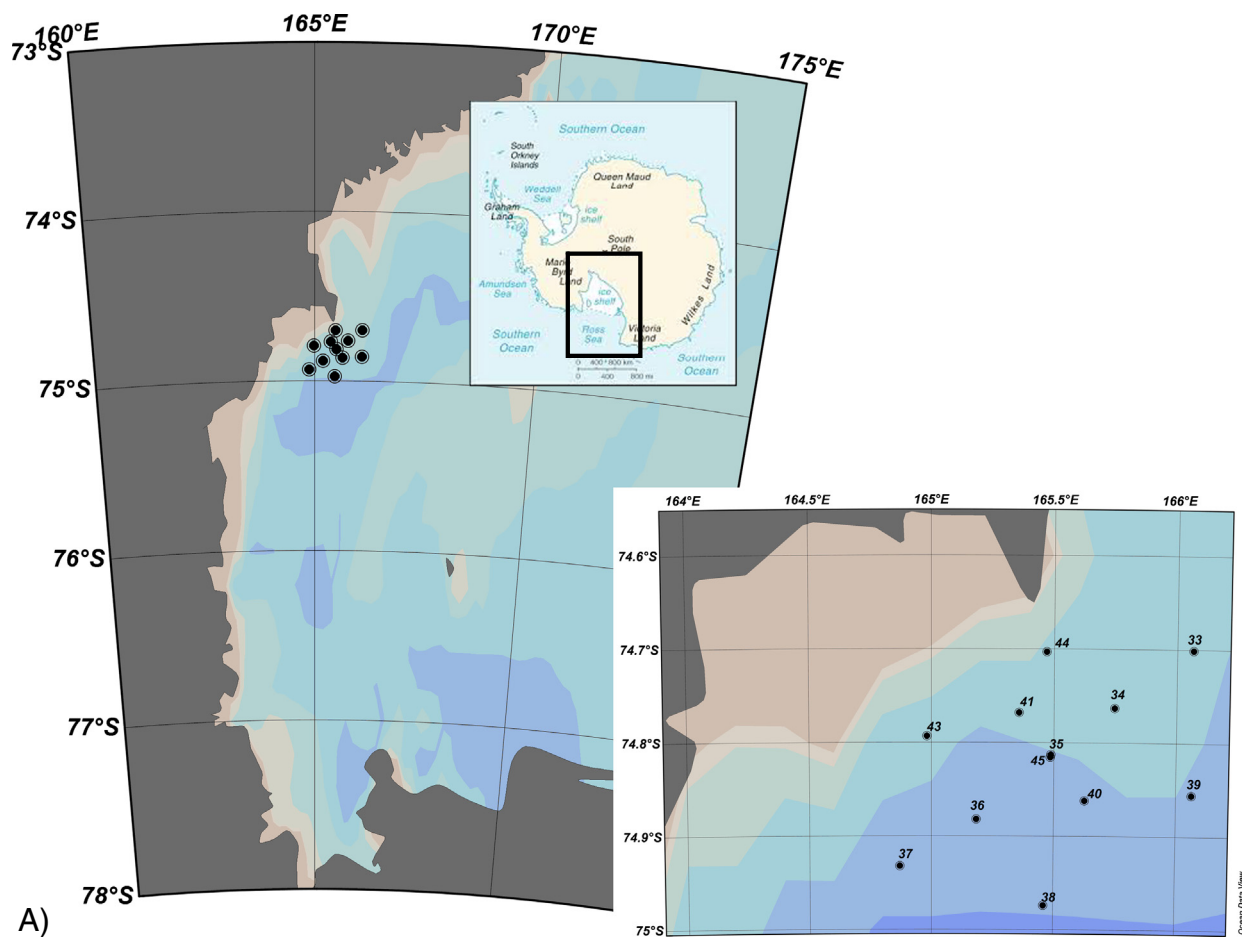

Fig. 1. A) Map of the sampling stations from 26th to 28th January 2014. Station 35 was revisited after 24 h (station 45). The insets show the region of study inside the Ross Sea. The map was drawn with Ocean Data View software (Schlitzer, 2015). B) The position of the sampled stations (blue circles) with respect to the MODIS SST. C) The position of the sampled stations (blue circles) with respect to the MODIS surface Chl-a. Satellite data retrieved from Aqua and Terra satellites level-2 data at 1 km resolution, relative to 25th (left) and 28th (right) January 2014.
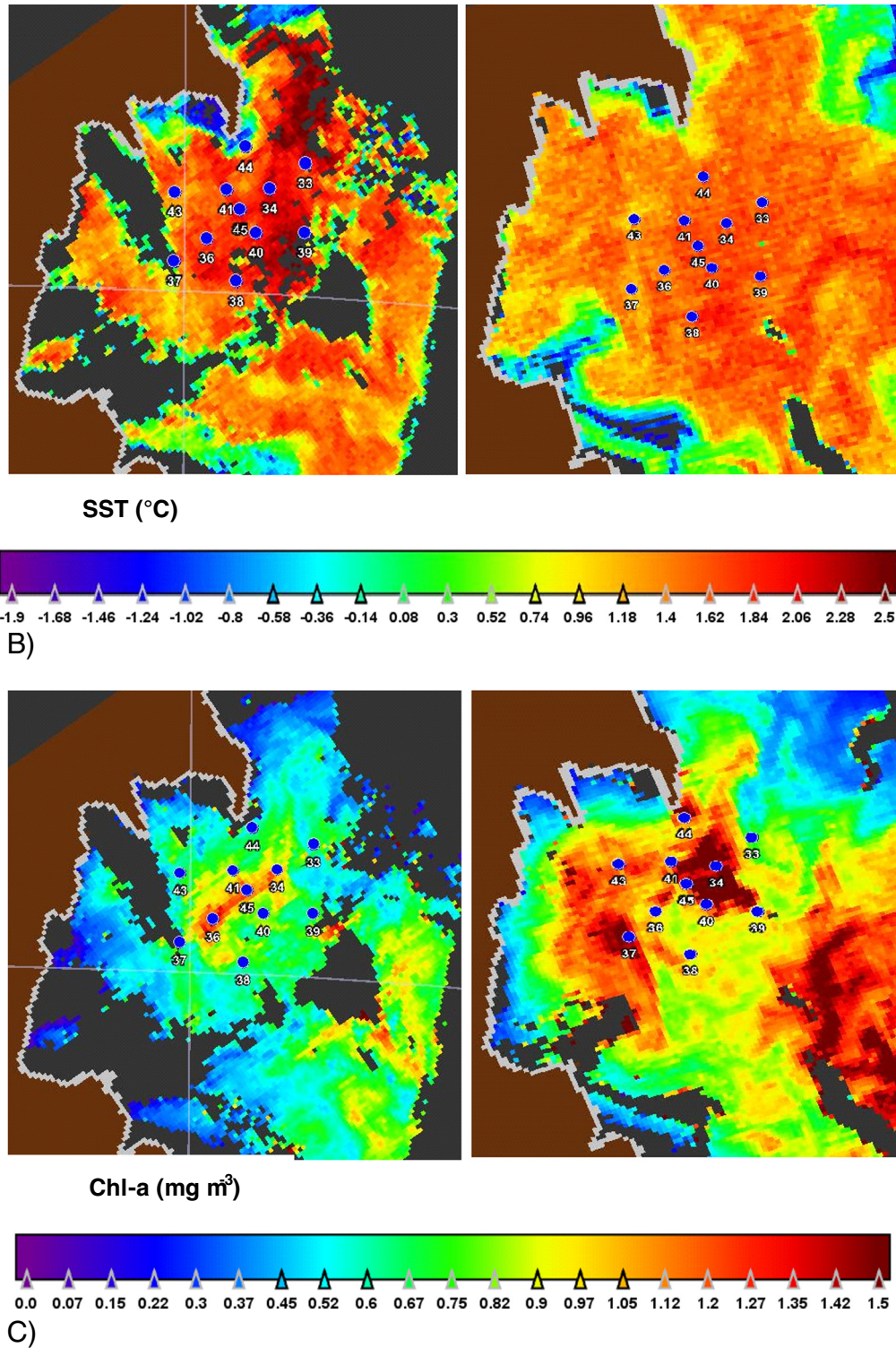
SST (°C)

-1.9 -1.68 -1.46 -1.24 -1.02 -0.8 -0.58 -0.36 -0.14 0.08 0.3 0.52 0.74 0.96 1.18 1.4 1.62 1.84 2.06 2.28 2.5

B)

Chl-a (mg m^3)

0.0 0.07 0.15 0.22 0.3 0.37 0.45 0.52 0.6 0.67 0.75 0.82 0.9 0.97 1.05 1.12 1.2 1.27 1.35 1.42 1.5

C)

Fig. 1 (*continued*).

The sea–air CO_2 flux (F, in mmol m^{-2} d^{-1}) was computed as

$$F = ks(\Delta pCO_2) \tag{1}$$

where k is the CO_2 gas transfer velocity (cm h^{-1}), s is the solubility of CO_2 (mol kg^{-1} atm^{-1}) and ΔpCO_2 is the difference between the pCO_{2SW} and the pCO_{2atm}. Ship-based wind speed data at 10 m height (u) were used for the calculation of the gas transfer velocity (k) according to Wanninkhof (1992):

$$kCO_2 = 0.31u^2(660/ScCO_2)^{0.5} \tag{2}$$

where $ScCO_2$ is the Schmidt number for CO_2.

2.5. Ancillary data

Melt water percentage in the surface layer (MW%) was calculated from the difference between the salinity measured at the surface (S_{meas}) and at greater depth (S_{deep}, i.e., 200 m), and assuming an average sea-ice salinity of 6 (Rivaro et al., 2012, 2014):

$$MW\% = \left(1 - \frac{S_{meas} - 6}{S_{deep} - 6}\right) * 100. \tag{3}$$

Mixed layer depth (MLD) was estimated to be the depth at which an increase of in situ density (σ_t) > 0.05 over 5 m was observed.

3. Results

3.1. Physical properties

The θ/S diagram (Fig. 2) shows the presence of characteristic Ross Sea water masses. The surface layer from 30 to 50 m is occupied by a local expression of Antarctic Surface Water (AASW). AASW is the relatively light surface water showing a large range of temperatures (~ − 1.8 °C to + 1 °C) and salinities (from < 34.00 to ~ 34.50), because it lies at the air/sea-ice interface (Orsi and Wiederwohl, 2009). In our study indeed, the AASW core was found at about 50 m, with salinity values close to 34.6 and potential density values lower than 27.9 kg m^{-3}. These values are slightly saltier, colder and denser than expected for typical AASW and more similar to Modified Circumpolar Deep Water (MCDW) core parameters. However, O_2 content (see Fig. 2) shows high oxygen concentrations, precluding the presence of MCDW. The differences from AASW typical values are probably due to

local conditions. Summer insulation and ice melt are also responsible for the increased temperatures and lower salinities of the surface layer (shallower than 30 m).

The variability observed in surface layers is not found in the intermediate and deep layers (from 100 to 1000 m) that are occupied by High Salinity Shelf Water (HSSW) and Ice Shelf Water (ISW). HSSW is characterized by a salinity maximum greater than 34.7, potential temperature near the freezing point and potential density greater than 27.9 kg m^{-3} (Budillon et al., 2003; Rivaro et al., 2014). The coldest water mass identified during the experiment is the local ISW (Budillon and Spezie, 2000) with potential temperatures below the freezing point and salinity of about 34.7.

A frontal zone was observed along with a convergence (black dashed line in Fig. 3) between two circulation systems and is characterized by abrupt variation of temperature and salinity (see also Section 4.3, Fig. 9A and B). Fresh and cold water masses, possibly influenced by melting and then driven offshore by eastwards currents, are only observed at stations 41, 43, 44 on the western side of the front. Stations 34 and 35/45 show T and S characteristics intermediate between coastal and eastern water masses. The existence of this front is also evident in terms of U and V components of the observed currents (Fig. 9C and D). The general current pattern is sketched in Fig. 3, whereas a specific section will be discussed in Section 4.3. LADCP measurements reveal the presence of a significant gradient across the frontal line as well as an inversion of resulting current directions just east of station 35/45, as confirmed by the analysis of geostrophic currents derived from CTD data (not shown). Finally, the absence of any upwelling signal (see Section 4.3) associated with the presence of a cyclonic circulation in the middle of the study area seems to confirm the existence of a meridionally oriented front near 165.6°E.
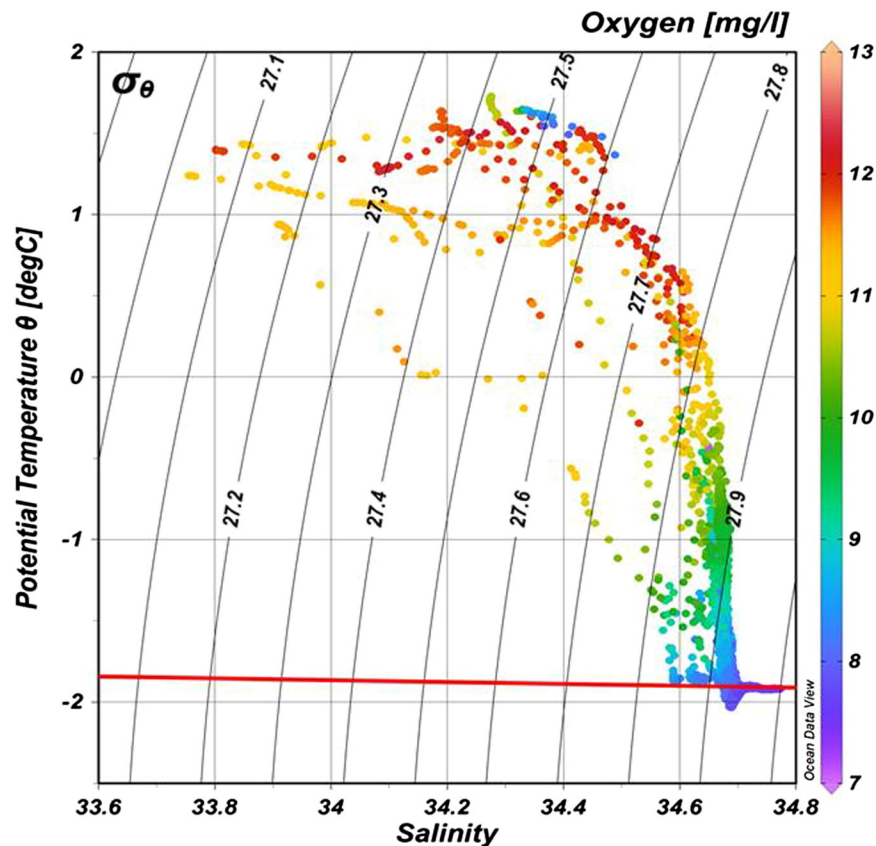

Fig. 2. Potential temperature/salinity (θ/S) diagram of the sampled stations. The color scale refers to dissolved oxygen concentration (mg L^{-1}). The red line indicates the surface freezing point at different salinity values.
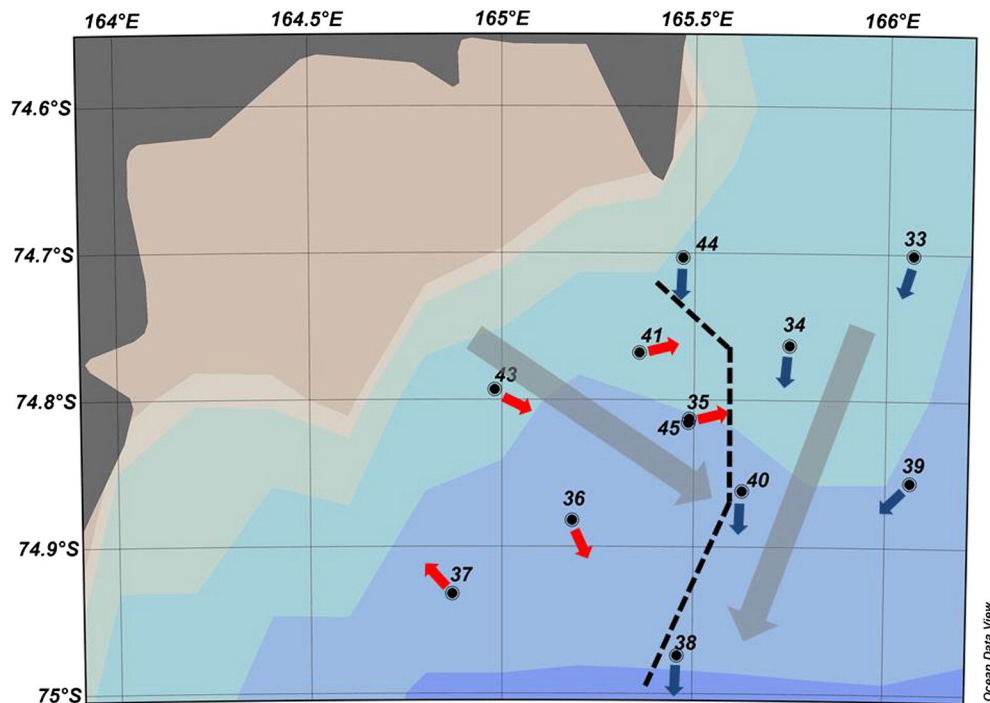
Fig 3. A simplified scheme of the main currents acting in the study area during RoME 2. The dimensionless blue and red arrows represent the integrated direction derived by LADCP observations collected every 10 m from surface to maximum reached depth. The over imposed dashed line and the gray arrows show the position of the described frontal structure and the main current pattern, respectively.

3.2. Chemical and biological properties

The A_T and the C_T (Table 1) ranged between 2313 and 2365 μmol kg^{-1} and 2017 and 2266 μmol kg^{-1}, respectively, with the lowest values at the surface in agreement with previous Ross Sea data (Joint Global Ocean Flux Survey (JGOFS) Antarctic Environment and Southern Ocean Process Study (AESOPS) in the Ross Sea http://usjgofs. whoi.edu/jg/dir/jgofs/southern/nbp97_8/; http://usjgofs.whoi.edu/jg/ dir/jgofs/ southern/nbp97_3/; Sandrini et al., 2007; Rivaro et al., 2014; DeJong et al., 2015). The pH ranged between 8.42 and 7.96, with the highest values at the surface and decreasing values with depth. As expected, C_T and A_T correlate significantly and positively with the distribution of salinity ($r = 0.79$ and 0.92, respectively). A strong positive correlation was observed between the A_T and C_T ($r = 0.61$, $n = 61$), and a negative correlation was found between pH and C_T ($r = -0.98$, $n = 61$). The surface pCO_{2SW} values were well below the atmospheric values (cf. Table 3), ranging from 146 to 236 μatm, and a general increase was observed with depth to 450 μatm at 200 m. They are comparable but slightly lower than those reported in the western region of the Ross Sea (DeJong et al., 2015). All of the samples are oversaturated with respect to calcite and aragonite, but near corrosive level of Ω_{Ar} (~1.0) is found only in the deepest samples collected at stations 39 and 43 (1080 and 775 m, respectively). The O_2 concentration decreased from the surface to 200 m at each station. In some stations (34, 36, 41, 43 and 45), values in the upper 20 m (from 10.4 to 12.6 mg L^{-1}) were above the saturation level ($104 - 113\%$).

Total phytoplankton biomass Chl-a at the surface ranged from 0.90 to 2.56 mg m^{-3} (average 1.52) with integrated values ranging from 115 to 371 mg Chl-a m^{-2} (average 232) (Table 2). The surface Chl-a concentrations were correlated ($r^2 = 0.98$) with those throughout the top 0–100 m only for the stations 34, 35, 36, 43 and 45. Chl-a concentrations within the water column varied between 0.58 and 3.79 mg m^{-3}, with the highest value found at station 41 at 30 m. The highest values of Chl-a were found in the layer between 20 to 50 m. The percentage contribution of different size classes to phytoplankton biomass showed

an evident predominance of the micro-phytoplankton fraction (>20 μm) of about 73% (± 11). The variability of major function groups (CHEMTAX analysis) along the water column during the entire sampling period is reported in Fig. 4. The maximum diatom biomass occurred only above 25 m, whereas haptophytes dominated the phytoplankton communities below 30 m. The taxonomic analyses as well as CHEMTAX analysis underline the dominance of haptophytes and diatoms that make up 90% of the phytoplankton assemblages. The haptophytes were represented primarily by colonial *Phaeocystis antarctica* while *Fraglariopsis* spp., *Pseudo-nitzschia* spp. and *Cylindrotheca closterium* were the most abundant diatom species. All stations were characterized by a similar vertical structure of phytoplankton. It is important to note that the diatom assemblages in the upper layer of stations 33, 34, 41, 43, 44, 45 were constituted by large cells with empty frustules and in senescent status.

The phytoplankton physiological status varied throughout the water column. The maximum quantum yield (F_v/F_m) in the upper layer changed from 0.19 to 0.49 (mean 0.33 ± 0.07). In the deep layer (below 30 m), the maximum quantum yield varied from 0.22 to 0.75 (mean 0.42 ± 0.13); the highest value was detected at 35 m at station 45 where *P. antarctica* represents the 97% of cell counts (Light Microscope, LM) of phytoplankton assemblages. Additionally, it is worth to mention the F_v/F_m value of 0.52 observed at 80 m in station 43, where *P.antarctica* represents the 98% of cell counts.

4. Discussion

4.1. Mesoscale drivers affecting the carbonate system chemistry in surface water

The carbonate system properties in surface water exhibited mesoscale variability with a horizontal length scale of about 10 km, which could be connected to both physical and biological forcing. The melting of the sea ice plays an important role in controlling the summer AASW physical and chemical features in the Ross Sea. The RoME cruise was

Table 1
Carbonate system and O_2 data from RoME 2 stations.

Station	Depth (m)	AT (µmol kg^{-1})	H	pCO2 (µatm)	CT (µmol kg^{-1})	Ω Calcite	Ω Aragonite	O_2 mg L^{-1}	O_2 % sat
33	2	2351	8.25	236	2135	3.7	2.3	12.6	114
	18	2354	8.06	379	2234	2.3	1.4	9.4	79
	40	2352	8.09	348	2222	2.4	1.5	9.9	83
	80	2354.	8.05	384	2238	2.2	1.4	9.9	83
	120	2356.	8.06	378	2239	2.2	1.4	9.9	82
	135	2358	8.01	426	2257	2.0	1.2	9.2	77
	400	2355	7.98	445	2259	1.8	1.1	9.4	79
34	2	2337	8.42	148	2037	5.0	3.1	12.5	112
	10	2342	8.37	172	2070	4.5	2.8	12.3	111
	30	2365	8.24	243	2164	3.4	2.2	11.4	99
	60	2359	8.14	309	2204	2.8	1.7	10.7	91
	220	2352	8.15	292	2198	2.6	1.7	9.2	76
35	2	2350	8.40	156	2058	4.9	3.0	12.0	108
	35	2371	8.24	242	2168	3.5	2.2	11.5	101
	70	2357	8.10	338	2219	2.5	1.6	10.3	87
	110	2353	8.05	390	2238	2.2	1.4	10.0	84
	200	2349	8.00	428	2250	1.9	1.2	9.2	77
36	2	2333	8.32	194	2086	4.1	2.6	11.6	104
	10	2345	8.35	179	2081	4.4	2.8	12.0	108
	20	2343	8.32	196	2109	3.9	2.5	12.1	105
	40	2358	8.21	263	2173	3.2	2.0	11.5	100
	160	2350	8.00	431	2252	1.9	1.2	9.3	78
37	2	2332	8.38	165	2060	4.5	2.8	9.1	75
	25	2357	8.23	249	2164	3.3	2.1	11.8	105
	60	2350	7.96	479	2266	1.8	1.1	11.3	98
	80	2349	8.00	439	2253	1.9	1.2	9.2	77
	200	2344	8.00	430	2247	1.9	1.2	9.2	76
38	2	2315	8.34	185	2064	4.2	2.6	11.6	104
	37	2362	8.19	277	2184	3.1	1.9	11.1	97
	50	2351	8.06	377	2231	2.3	1.4	10.0	84
	100	2353	8.00	436	2256	2.0	1.2	9.0	75
	200	2339	8.00	431	2242	1.9	1.2	8.5	71
39	2	2349	8.30	206	2109	4.0	2.5	11.3	102
	20	2351	8.26	230	2136	3.6	2.3	11.0	98
	50	2351	8.14	306	2193	2.8	1.8	10.8	94
	200	2333	7.98	454	2243	1.8	1.1	8.9	74
	1080	2347	7.97	420	2248	1.6	1.0	9.2	77
40	2	2363	8.35	181	2097	4.4	2.8	12.1	109
	30	2365	8.20	268	2180	3.2	2.0	11.2	98
	60	2347	8.11	337	2207	2.5	1.6	10.5	89
	100	2342	7.99	443	2247	1.9	1.2	9.2	76
	200	2342	7.99	435	2246	1.9	1.2	9.1	75
41	2	2342	8.37	172	2072	4.5	2.8	12.2	109
	20	2349	8.35	181	2087	4.4	2.7	12.4	111
	30	2349	8.27	221	2130	3.7	2.3	11.7	103
	80	2344	8.04	396	2232	2.2	1.4	9.6	81
	200	2358	7.98	451	2266	1.9	1.2	9.3	77
43	2	2316	8.38	165	2044	4.5	2.8	11.8	106
	20	2338	8.33	188	2091	4.1	2.6	12.0	107
	40	2364	8.21	261	2175	3.2	2.0	11.6	101
	200	2352	8.01	423	2251	2.0	1.2	9.2	76
	775	2362	7.97	430	2264	1.7	1.1	9.4	78
44	2	2313	8.42	146	2017	4.9	3.1	12.6	113
	30	2360	8.10	342	2223	2.5	1.6	10.4	88
	100	2358	8.02	420	2254	2.0	1.3	9.7	81
	188	2351	8.02	415	2247	2.0	1.3	9.4	78
45	2	2341	8.34	186	2083	4.3	2.7	11.9	102
	10	2349	8.35	178	2083	4.4	2.8	12.1	109
	25	2360	8.33	188	2106	4.2	2.7	10.5	94
	100	2364	8.06	376	2244	2.3	1.4	10.0	83
	200	2352	8.01	419	2250	2.0	1.2	9.3	77
	701	2358	8.01	398	2250	1.8	1.2	9.5	79

characterized by largely ice-free conditions over most of the southern Ross Sea. Solar heating encourages sea ice melting with the formation of shallow UML. To evaluate the effect of the sea ice melt on the physical and chemical properties at the surface, we calculated the percentage of melt water (MW%) which varied from 0.9% (in station 40, where the salinity reached the highest surface value of 34.43) to 3.1% (at station 44, where the lowest salinity of 33.78 was measured) with a mean value of 2.1%. The UML depth and irradiance are two of the main factors affecting phytoplankton and its dynamics, as the presence of a shallow pycnocline keeps phytoplankton in the euphotic layer (Arrigo et al., 1999; Mitchell and Holm-Hansen, 1991). The UML depth plays a role in determining the dominant species in the Ross Sea area. In fact, diatoms are usually most abundant in areas of shallower mixed layer depth and more stratified waters (Arrigo, 2007; Arrigo et al., 1999; Smith et al., 2010). A very shallow UML was calculated for the sampled stations (16 ± 5 m), comparable to other data reported for coastal areas

Table 2
Mean values of surface and integrated Chl-a in the $0 - 100$ m layer.

Station	mg Chl a m^{-3}	mg Chl a m^{-2}
33	1.13	115
34	2.56	371
35	1.95	320
36	1.22	246
37	1.61	133
38	0.90	226
39	1.00	166
40	1.17	202
41	1.62	212
43	1.52	277
44	2.31	235
45	1.30	276

of the Ross Sea (Massolo et al., 2009; Saggiomo et al., 2002). The smallest value occurred at station 44 (7 m), whereas the deepest was at stations 35 and 39 (23 and 24 m, respectively). Therefore, when our survey took place, the area was characterized by hydrographically favorable conditions for diatom growth, as it was confirmed by the CHEMTAX analysis. The phytoplankton distribution we observed (maximum diatom biomass above 25 m and haptophytes dominating the phytoplankton communities below 30 m) is in agreement with Arrigo et al. (1999) and Annett et al. (2010), who suggested that deep mixing promotes growth of *P. antarctica* as a result of its ability to adapt to a large range of irradiance levels (Arrigo et al., 1999). Conversely, a stratified water column favors diatoms, which are better adapted to higher light levels, such that they accumulate in stratified and in shallow-mixed layer regions, such as typically are found near ice edges (Arrigo et al., 1999, 2000; Goffart et al.;, 2000; Smith et al., 2010).

Wind speed is an important factor in controlling the energy that is transferred into the ocean and results in vertical mixing (Smith et al., 2011b), therefore we could expect slightly deeper UML where highest wind speed are recorded. However, in our study, no significant differences of the UML were found between the investigated stations depending on the wind speed. On the contrary, the significant negative correlation between MW% and UML (Pearson's $r = -0.76$, $p = 0.05$) emphasizes the importance of ice melt in inducing stratification.

The MW% also co-varied significantly and negatively with surface A_T (Pearson's $r = -0.96$, $p = 0.05$) and C_T (Pearson's $r = -0.72$, $p = 0.05$), consistent with the fact that the distribution of surface A_T and C_T is controlled by factors linked to salinity. Therefore, the addition of low salinity melt water results in a dilution of the A_T and C_T. The A_T–C_T relationship can be used to determine whether the cause of the variability is due to processes such as photosynthesis–respiration or CaCO$_3$ production–dissolution (Bates et al., 1998). To assess this, surface

and subsurface (10–30 m) A_T and C_T were normalized (A_T N and C_T N) to a constant salinity of 34.50 (roughly the average salinity of the Ross Sea upper water column) to remove the effects of dilution from the melting sea ice (Dunbar et al., 2003). Photosynthesis and respiration can influence C_T but not A_T, whereas CaCO$_3$ production–dissolution acts on both C_T and A_T at a ratio ranging between 1:1 and 1:2, depending on the ratio of organic carbon production to CaCO$_3$ production (Robertson et al., 1994). A_T N and C_T N ranged from 2344 to 2373 μmol kg^{-1} and from 2063 to 2225 μmol kg^{-1}, respectively. A_T N variability was smaller (29 μmol kg^{-1}) than C_T N variability (162 μmol kg^{-1}) and was linearly related to C_T N as follows:

$$A_T N = -0.118 + 2612\, C_T N \quad (r^2 = 0.57) \tag{4}$$

This relationship indicates that photosynthesis–respiration, rather than CaCO$_3$ production–dissolution, controls C_T variability in surface and subsurface water. In fact, the A_T N:C_T N ratio is close to the value found by Bakker et al. (2008) for the Weddell Sea and consistent with data reported by Anderson and Sarmiento (1994) for organic matter production. Furthermore, the phytoplankton role in determining C_T concentration is confirmed by the high pH in corresponding to the low C_T N values, as a result of the displacement of the carbonate equilibrium related to CO$_2$ consumption (Fig. 5A) and O$_2$ evolution (Fig. 5B) and by the negative correlation between Chl-a and C_TN.

Chl-a was used to investigate the role of biological CO$_2$ drawdown on the variability of the carbonate system and Ω. Generally, the presence of water masses connected to sea-ice melting results in low Ω due to dilution of [CO$_3^{2-}$] (Mattsdotter Björk et al., 2014). Nevertheless, our data suggest that biological activity was the main cause for the observed Ω$_{Ar}$ distribution. In fact, a strong positive correlation was observed between Ω$_{Ar}$ and Chl-a ($r = 0.77$, $n = 16$) at the surface and subsurface, with the highest Ω$_{Ar}$ values (3.1 and 3.0) in those stations characterized by the highest Chl-a and by the shallowest UML. CO$_2$ is removed in photosynthesis, leading to higher CO$_3^-$, higher Ω$_{Ar}$, and increased pH where the highest values of Chl-a were recorded. A seasonal cycle of Ω$_{Ar}$ in the Ross Sea surface waters has been reported, with increasing values during the summer months, because of the dominant control exerted by photosynthesis on the C_T (DeJong et al., 2015; McNeil et al., 2010). Our Ω$_{Ar}$ values (2.8 ± 0.2) are comparable to those reported by McNeil et al. (2010) during the summer months (3–4) and higher than those found by DeJong et al. (2015) for the western Ross Sea (1.94 ± 0.18) at the end of summer, when the C_T concentrations would have already increased. The effect of biological processes on the Ω$_{Ar}$ has been reported over large spatial and temporal scales (DeJong et al., 2015; Mattsdotter Björk et al., 2014), but mesoscale variations such as those we found have never been reported. Based on
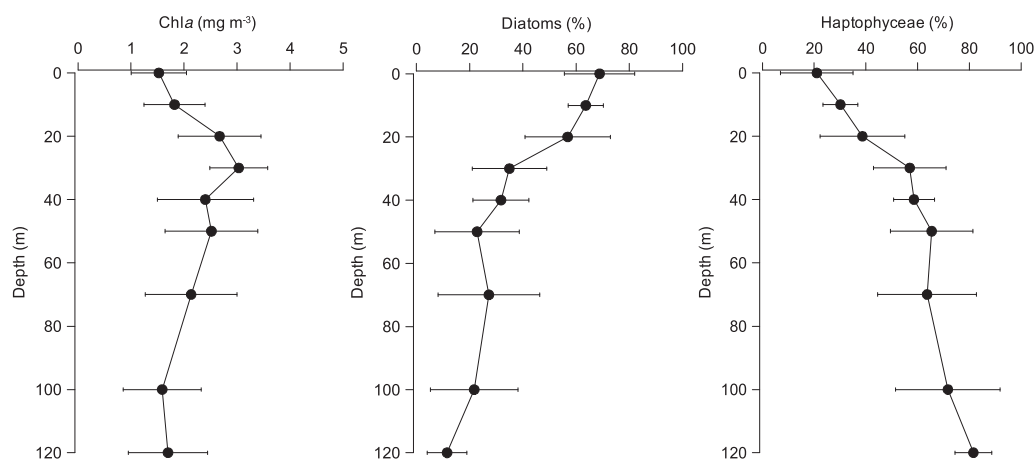

Fig. 4. Vertical profiles of mean and standard deviation of the total biomass (Chl-a concentration) and of the principal functional groups (percentage contribution of diatoms and haptophytes) to the phytoplankton community by CHEMTAX analysis in all stations.
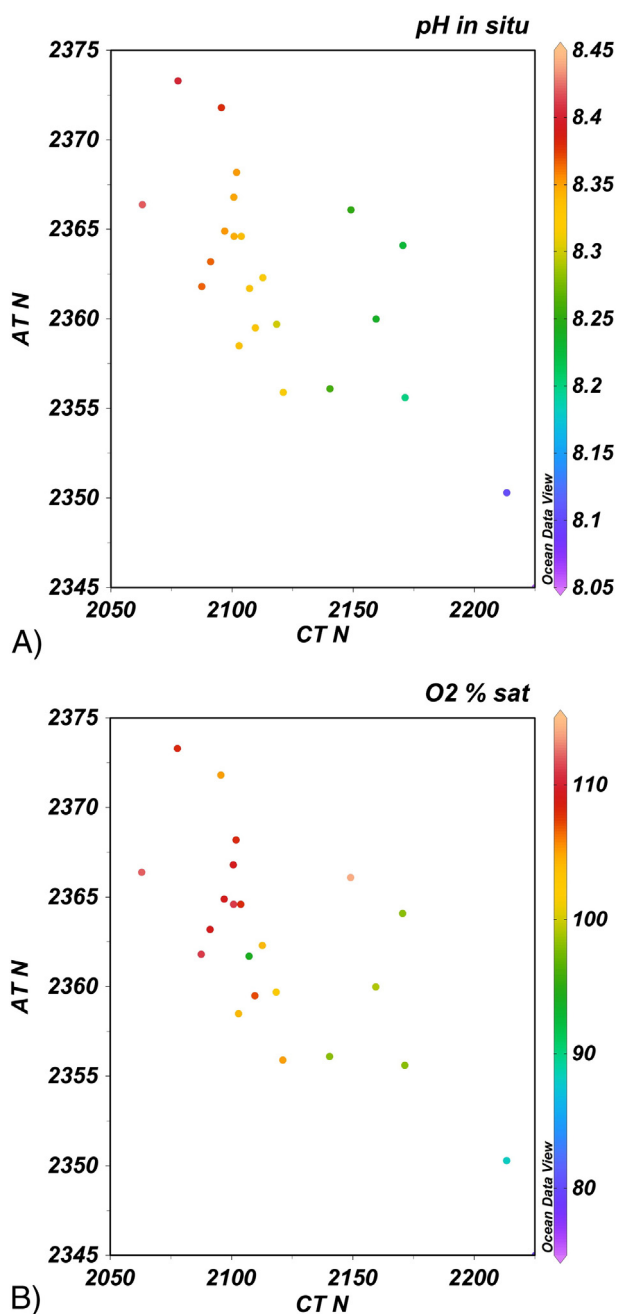
Fig. 5. Scatter plot of 0–30 m layer normalized total alkalinity (A_T N) and normalized total inorganic carbon (C_T N). The color scale refers to pH values (A) and O_2 saturation percentage (B).

these results, the distribution of the carbonate system parameters in surface waters was largely controlled by phytoplankton activity.

Therefore, the dilution due to the melting sea ice had a small direct effect on Ω_{Ar}, but also an indirect effect as well, given its importance on the UML and the stability of the water column.

4.2. Mesoscale physical and biological forcing on the local air–sea CO_2 flux

Surface pCO_{2SW} is controlled by SST, biological uptake of CO_2, remineralisation of organic carbon back to CO_2, air–sea CO_2 exchange and mixing with CO_2-rich waters from depth (Arrigo and Van Dijken, 2007). As surface waters stratify and the phytoplankton bloom intensifies during summer, the production of organic matter in the surface waters consumes C_T and makes pCO_{2SW} decrease, potentially enhancing the uptake of CO_2 from the atmosphere. Surface pCO_{2SW} data were

below the atmospheric mean and had a large spatial variability (146–236 µatm), whereas the measured pCO_{2atm} varied little (from 391.7 to 392.2 µatm). The pCO_{2SW} values show a small-scale heterogeneity and are comparable to those reported for the Ross Sea surface waters during the summer season (Bates et al, 1998; Sweeney, 2003; Tortell et al., 2011). Few recent articles have quantified the length scales of surface gas and hydrographic variability in the Ross Sea using high spatial resolution measurements (Hales and Takahashi, 2004; Tortell et al., 2011). In particular, our data are consistent with the analysis of length-scale dependent pCO_2 variability in surface waters of the Ross Sea polynya carried out by Tortell et al. (2011) who demonstrated that much of the spatial variance in surface water gasses occurred at scales of < 20 km. Therefore, the computed air–sea CO_2 (ΔpCO_2) gradient was negative, corresponding to a net transfer of CO_2 from the atmosphere to the ocean. The solubility is one pivotal mechanism in controlling the oceanic uptake of CO_2 across much of the Southern Ocean, but in geographically limited areas where intense biological production occurs, such as polynyas and other marginal ice zones or coastal areas, biological processes become important for transferring CO_2 from the atmosphere to the ocean (Arrigo et al., 2008; Bates et al., 1998; Laika et al., 2009; Rivaro et al., 2014). However, it should be mentioned that even though disequilibria occur, this does not mean that atmospheric CO_2 enters quickly the ocean, as the time scale of air–sea exchange relative to drawdown are different.

The greatest air–sea CO_2 disequilibrium occurred at stations 34 and 44 (− 241.6 µatm and − 243.4 µatm), corresponding to O_2 supersaturation (112–113%) and high pH_T values (8.42 at both stations). MODIS SST and Chl-a maps indicated the occurrence of substantial production. Specifically, satellite images captured a few hours before our sampling showed an inhomogeneous chlorophyll distribution, with filaments characterized by chlorophyll concentrations higher (~1.4 mg m^{-3}) than the surrounding water (~0.4–0.5 mg m^{-3}, cf. Fig. 1C). In particular, starting from 25th January higher Chl-a concentrations were observed at stations 34 to 36. During the following days this increase in Chl-a concentration assumed a horseshoe shape. In situ fluorescence measurements were well correlated with satellite maps, despite the time and depth biases (Figs. 1C and 7E). The ΔpCO_2 pattern (Fig. 6A) parallels both satellite and in situ Chl-a measurements (Fig. 6B), which are the most common proxy of phytoplankton biomass. The phytoplankton assemblage results from a differential photosynthetic response of the two groups, with *P. antarctica* being able to photosynthesize (and presumably grow) more effectively at lower irradiances than diatoms (Arrigo et al., 1999). Also, the physiological state and light history of the phytoplankton communities have to be considered.

Most literature supports that maximum quantum yield (Fv/Fm) is a good indicator of phytoplanktonic physiological status (Franklin et al., 2009; Petrou et al., 2011; Russo et al., 2015; Smith et al., 2011b). Recently, measurements of the efficiency of photosystem PS II have become widespread in biological oceanography to assess the physiological status of phytoplankton communities. Absolute values of PS II efficiency depend to some extent on the measuring system, but changes in PS II efficiency are assumed to reflect the 'photosynthetic health' of the phytoplankton community, and to be affected mainly by cellular acclimations to changing abiotic conditions (including nutrient availability, especially N and Fe) (Franklin et al., 2009; Russo et al., 2015; Smith et al., 2011b, 2013). This up-regulation of PS II was also previously reported in sub-Antarctic zones (in microcosm studies), where higher values were observed when phytoplankton was not Fe limited (Petrou et al., 2011; van de Poll et al., 2005). For the Ross Sea, Smith et al. (2013) reported that quantum yields of PS II were mostly higher in spring relative to summer, likely reflecting adaptations to lower irradiance in spring. Reduced Fv/Fm values (<0.4) were detected in the upper 30 m in both seasons, with maximum values (0.55) observed below the euphotic zone. Dominance of *P. antarctica* appears to be related to quicker photoacclimation to changing light environments, whereas diatoms were dominant in shallow summer mixed layers, which reflects their
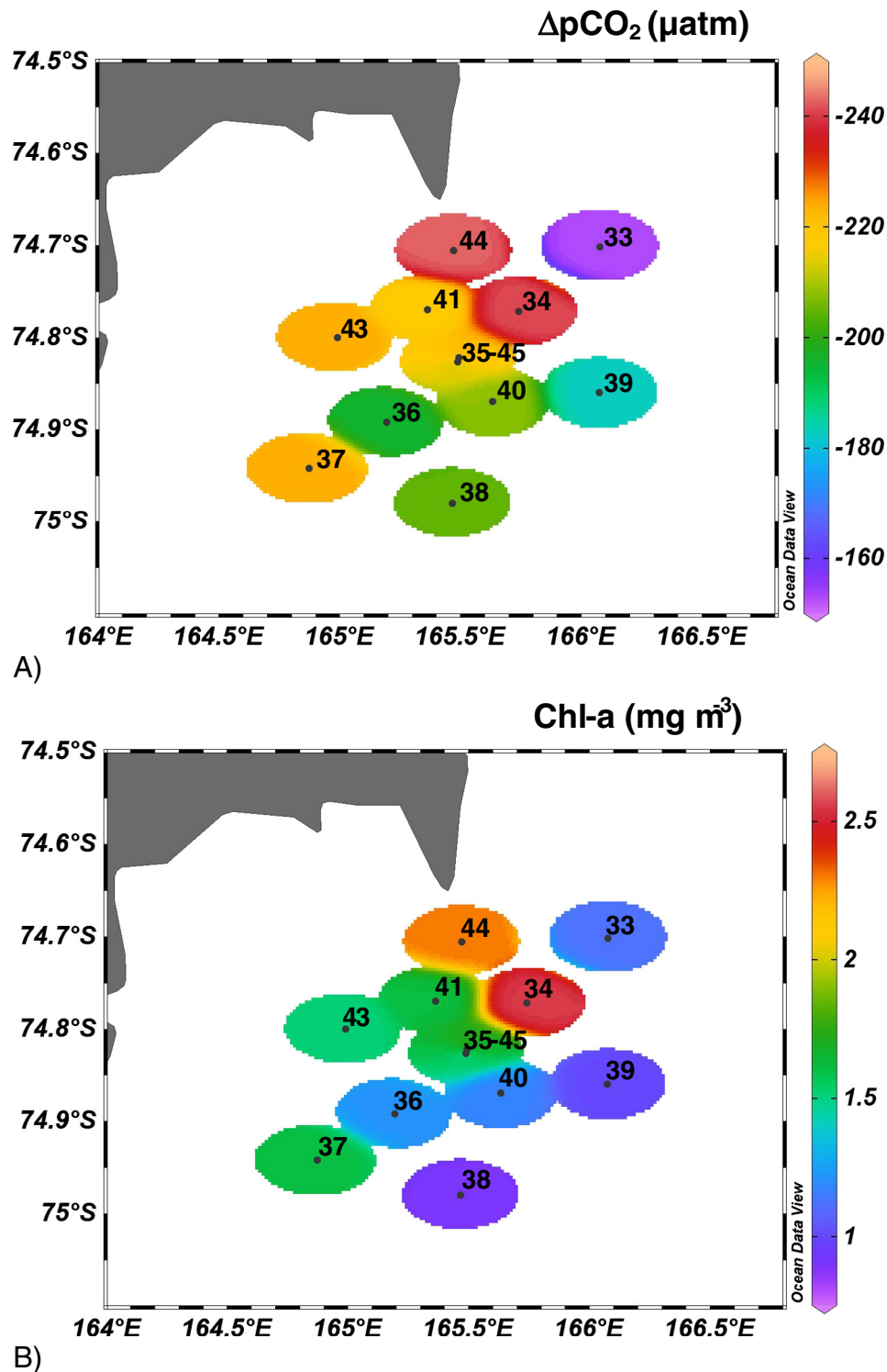
Fig. 6. Surface calculated ΔpCO_2 ($pCO_{2SW} - pCO_{2air}$) (µatm) (A) and Chl-a (µg L^{-1}) distribution (B).

improved photosynthetic capacity at high irradiance levels. Decline in the efficiency of PSII can be a function of the proportion of photosynthetically non-functional (dead) cells in the mixture. In fact, some field studies indicate that phytoplankton communities can contain large proportions of dead cells, and that these dead cells can, at times, be the most abundant fraction in surface waters (van Boekel et al., 1992; Veldhuis et al., 2001). Franklin et al. (2009) reported that in a number of species, mixtures in which 50% of the cells were dead had values of 0.5, similar to values often found in natural assemblages. Our

data show that in surface layer, where the large diatoms (from 50 to 150 µm) prevail, the mean Fv/Fm is 0.33, may be due to limiting factors. In fact, in several stations (33, 34, 41, 43, 44, 45) senescent diatoms were observed with empty frustules. Probably the empty frustules represent the end-member of Fe limitation (such as death cell). Fe limitation could be confirmed when data of Fe distribution and speciation collected in the framework of the RoME activities will be available.

The region overall acted as a sink of CO_2, with fluxes ranging from -0.5 ± 0.4 to -31.0 ± 6.4 mmol m^{-2} d^{-1} (Table 3). In particular,

Table 3
Atmospheric dry-pCO_2 (pCO_2 dry), atmospheric pCO_2 corrected to 100% humidity (pCO_2 wet), air–sea CO_2 gradient (ΔpCO_2) and calculated CO_2 flux (F).

pe	Wind speed (kts)	pCO_2 dry (μatm)	pCO_2 wet (μatm)	ΔpCO_2 (μatm)	F (mmol m^{-2} d^{-1})
33	21.7 ± 1.2	392.0	389.3	−153.2	−23.7 ± 2.8
34	19.6 ± 1.9	392.2	389.6	−241.6	−31.0 ± 6.4
35	11.4 ± 1.4	392.1	389.5	−233.6	−10.0 ± 2.6
36	13.3 ± 1.3	392.1	389.5	−195.9	−11.6 ± 2.4
37	10.5 ± 1.2	391.7	389.2	−224.3	−8.3 ± 2.1
38	8.7 ± 1.2	391.9	389.3	−204.6	−5.2 ± 1.5
39	8.3 ± 1.2	391.9	389.3	−183.1	−4.1 ± 1.3
40	4.7 ± 1.1	391.8	389.3	−208.1	−1.5 ± 0.8
41	2.8 ± 0.9	391.9	389.3	−217.6	−0.5 ± 0.4
43	12.8 ± 1.3	391.7	389.1	−224.4	−12.4 ± 2.6
44	11.2 ± 2.1	391.7	389.1	−243.0	−10.1 ± 4.2
45	14.5 ± 2.9	391.7	389.0	−203.5	−14.1 ± 6.2

the CO_2 air–sea flux at stations 38, 39, 40 and 41 was several times lower than those at the other stations. The mean value (-11.0 mmol m^{-2} d^{-1}) is comparable to those we already observed in the costal Terra Nova Bay (TNB) polynya (-12.7 and -15.4 mmol m^{-2} d^{-1}) during the 2008 CLIMA Project survey (Rivaro et al., 2014). The TNB polynya, which is smaller than the Ross Sea (RS) polynya, is also important in terms of productivity (Mangoni et al., 2004). Phytoplankton abundance is maximal in late December, declines thereafter, but a secondary peak appears in mid-February and it is dominated by diatoms (Tremblay and Smith, 2007). Unfortunately in CLIMA 2008 survey we could not directly confirm the phytoplanktonic drawdown on the pCO_2, distribution, because neither chlorophyll-a sampling nor fluorescence measurements were performed. Nevertheless, primary productivity calculated from Sea WiFS data referred to the investigated period allowed us to hypothesize that the phytoplanktonic drawdown made an important contribution in determining the pCO_2 in the upper AAWS. The large range in fluxes observed in the RoME 2 data is due to the significant short scale spatial variability of pCO_{2sw} depending on biological activities and wind speed encountered during the survey. We are conscious that the investigated area is not necessarily representative of the average coastal Ross Sea. Nevertheless, our data suggest that a high resolution analysis is needed to fully capture biogeochemical heterogeneity in coastal surface waters of the Ross Sea with particular regards the variance in air–sea CO_2 flux, which is important to predict future modifications in the carbonate system associated with climate change in the Ross Sea.

As wind speed is the main driver of the air–sea flux, together with the ΔpCO_2, the lowest fluxes were calculated for those stations characterized by the weaker hourly averaged winds. In contrast, the strongest CO_2 sink was observed at station 34 where low pCO_{2sw}, high pH_T and high wind speeds were observed. The revisited station (45) showed a slightly higher flux value with respect to its first sampling (station 35). Enhanced flux is mostly due to a higher wind speed, because no increase of photosynthetic biomass, as represented by Chl-a values, is found after 48 h. The importance of storms and their increased winds in the high-frequency (days) changes in CO_2 flux has been outlined by Arrigo and Van Dijken (2007), who investigated the air–sea exchange of CO_2 in the southwestern Ross Sea for 1997–2003 using the coupled ice atmosphere ocean (CIAO) model. The results showed that daily CO_2 flux reaches its seasonal maximum in February and March of each year, coinciding with the late summer increase in wind speed at a time when pCO_{2sw} is still well below atmospheric levels.

### 4.3. Influence of the mesoscale physical forcing on the vertical distribution.

Our sampling pattern allowed us to analyze the mesoscale variability along several NW–SE transects and one NE–SW section. After this, temperature and salinity data (stations 39, 40, 45, 41, 43) of a composed

longitudinal transect from surface to 200 m depth have been analyzed (Fig. 7A and B) T/S patterns highlight the presence of fresher and colder water in the western part of the transect (stations 43, 41, 45), as well as saltier and warmer water in the east (stations 39, 40). The deepening of colder water at station 45 and the maximum eastward extension of fresher water suggest that station 45 is next to a front, where a convergence between different waters could be located. Sections of the current zonal and meridional components confirm this hypothesis. An abrupt change in current direction is observed from station 41 to 40 both in terms of U (Fig. 7C) and V components (Fig. 7D), suggesting the presence of a convergence, possibly associated with the frontal position of station 45. Moreover, the calculation of geostrophic flow at several reference depths along the transect (not shown) confirms this pattern, showing a change in current directions associated with the front. Results from all transects lead us to construct the general circulation of the studied area as well as the front position (Fig. 3). The frontal zone near station 45 is reflected in the distribution of the carbonate system properties.

Higher pH and Ω_{Ar} and lower C_T and pCO_{2sw} occurred with the less saline waters of the western part of the section which occupied a thicker layer (30–40 m) than in the eastern part (Fig. 8). Here we also observed O_2 supersaturation and higher Chl-a concentration (Table 2). As previously stated, the surface phytoplankton was heavily dominated by diatoms relative to haptophytes, whereas *P. antarctica* was numerically dominant immediately following deepening of the mixed layer and determined the maximum values of Chl-a. Our data show that the physiological status of the phytoplankton was different along the water column. Indeed, PS II efficiency increased to 0.42 (± 0.13) in samples below 25 m simultaneously to an increase in the number of viable cells dominated by haptophytes that appeared well adapted to a low light conditions. The higher values of quantum yield were measured in the deep layer of stations 43 and 45 m, where *P. antarctica* represent the 98 and 97 %, respectively of phytoplankton assemblages in absence of limiting factors. A homogeneous distribution of C_T and other carbonate system properties was observed in waters below 50 m with an increasing trend with depth. This trend is due to an increasing pCO_{2sw}, which decreases the pH and the Ω_{Ar}.

The data demonstrate clearly that both physical and biogeochemical parameters vary with horizontal length scales lower than 40 km (approximately the length of the section). In particular, near the frontal zone at a given depth (~30 m) C_T vary by up to 50 μmol kg^{-1} in lateral distance of only 15 km. Also, the data show that a higher variability in all the biogeochemical parameters extend vertically as deep as 50 m. Thus, while the effect of the frontal zone on the carbonate properties was visible in the surface and sub-surface layer, it is less evident in the deeper layer. Therefore, mesoscale variability can significantly affect the carbonate system properties and their distribution throughout the water column. The resolution of these short length scale distributions provides insight into the biogeochemical dynamics which drive surface and subsurface variability. The observed patterns and interpretation of water column properties from our observations would have been markedly different if they were sampled at lower resolution.

Few studies of mesoscale variability in the Ross Sea have addressed short length scale biogeochemical variability, mainly of phytoplankton biomass (Kaufman et al., 2014; Smith et al., 2011b). Hales and Takahashi (2004) reported horizontal variability of meso- and submeso-scales ranging from several to 30 km in biologically mediated properties (i.e., pCO_2, O_2, C_T and nutrients) within the upper 140 m in the Ross Sea. Therefore, our variability is comparable to their observations with regards to the horizontal scale, whereas it is greater with regards the vertical scale. This difference could be ascribed to the sampled areas or to the sampling period. In fact our study sampled a coastal area in summer, characterized by a shallow UML, whereas Hales and Takahashi sampled the Ross Sea polynya in late spring, where deeper mixed layer depth can occur.
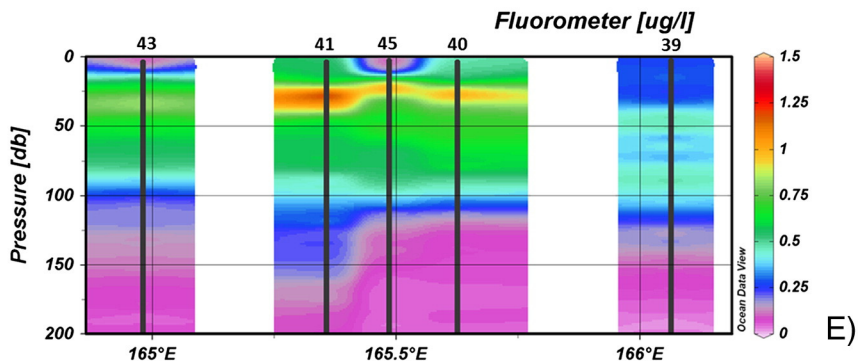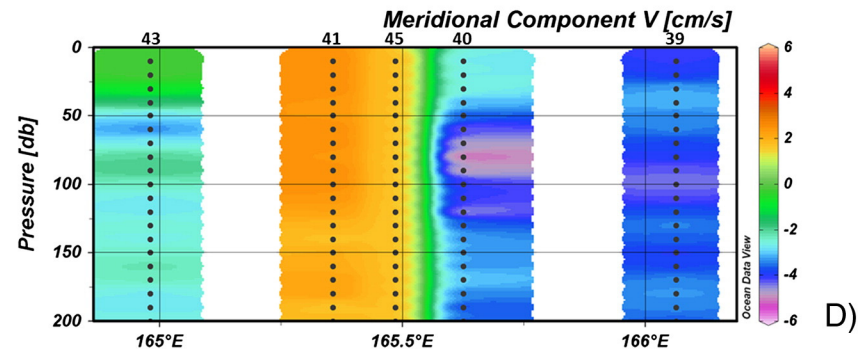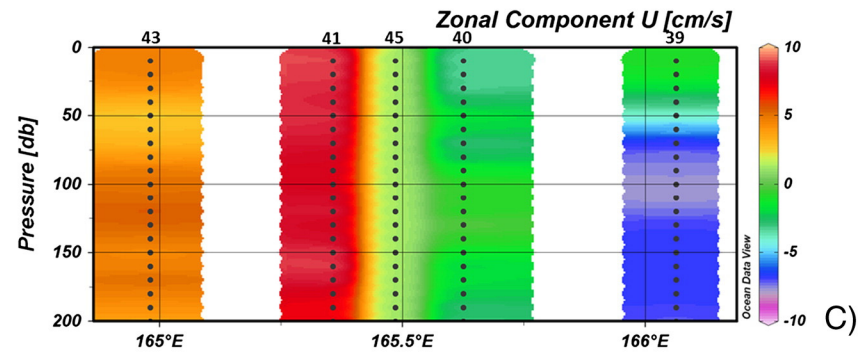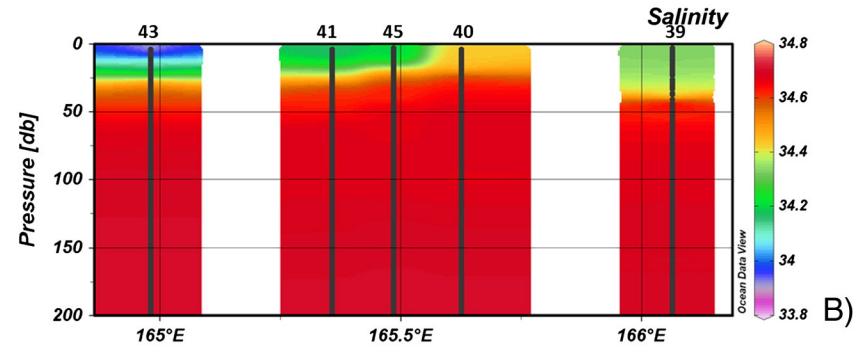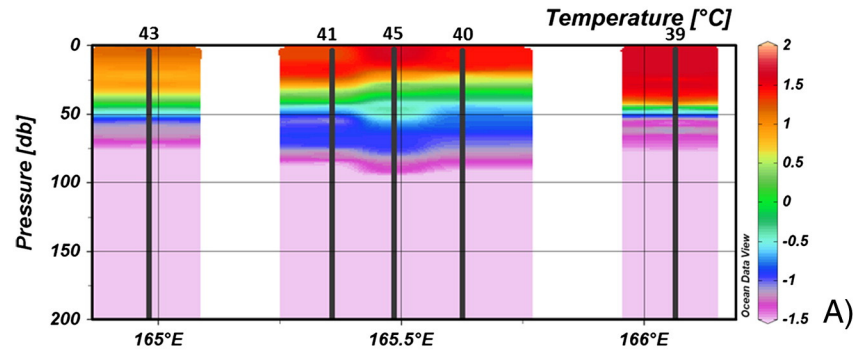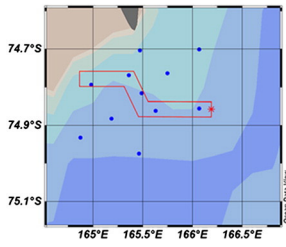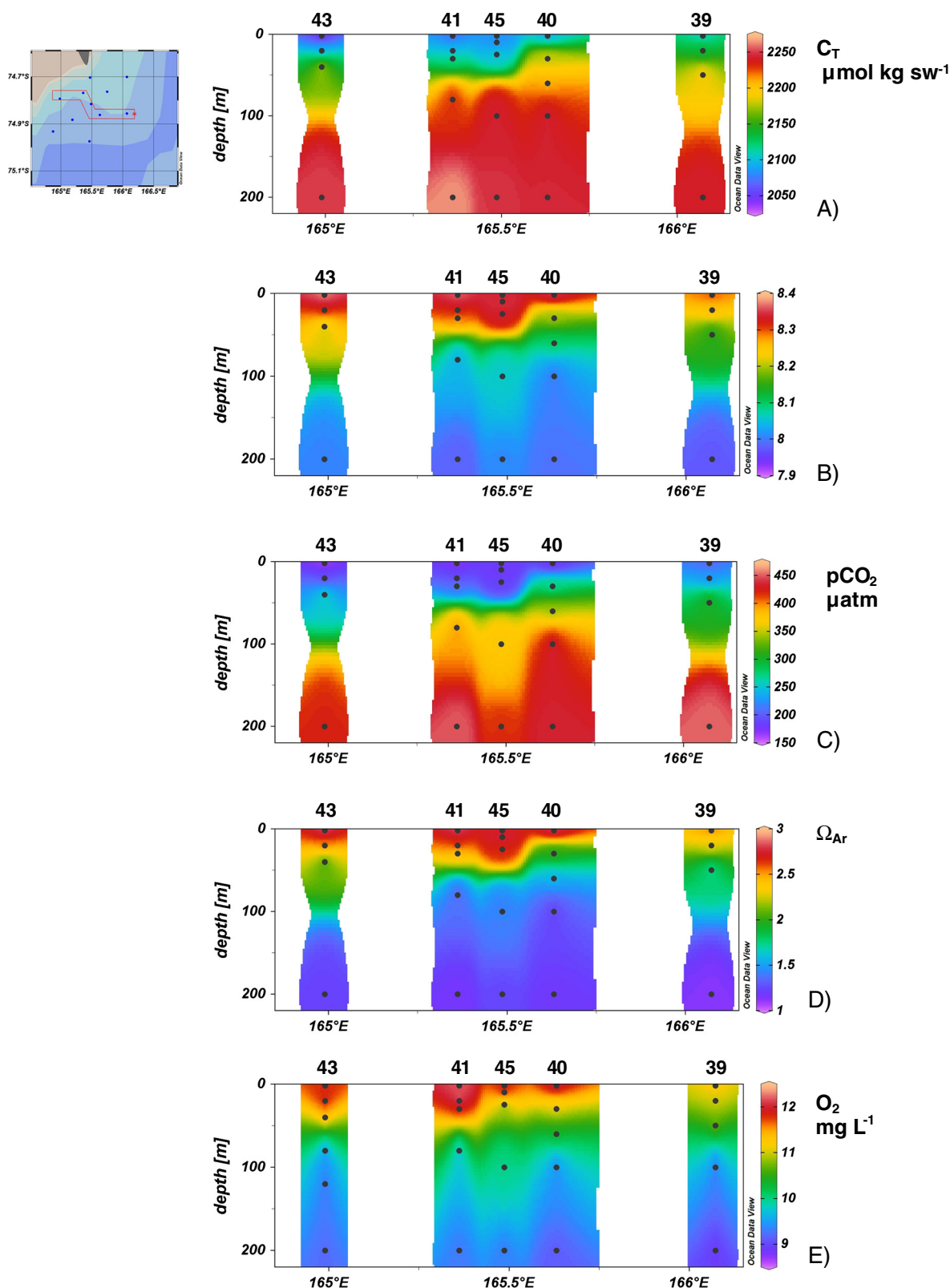
Fig.8. Sections of C$_T$ (A), pH (B), pCO$_2$ (C), Ω_{Ar} (D) and O$_2$ (E) across stations 39, 40, 45, 41, 43. The total section distance is 40 km and the maximum distance between consecutive stations is 12 km.

Fig. 7. Sections of temperature (A), salinity (B), zonal (C) and meridional (D) current components and in situ fluorometer (E) from surface to 200 m depth along the transect across stations 39, 40, 45, 41, 43. The total section distance is 40 km and the maximum distance between consecutive stations is 12 km.

5. Conclusion

The importance of mesoscale variability in the distribution of the carbonate system properties of the upper 200 m layers and in local air–sea CO_2 flux was investigated in a coastal area of the Ross Sea. The sampling strategy adopted by RoME using a combination of remote sensing and high resolution ship measurements, allowed us to describe environmental dynamics at a short length resolution. Therefore, it could represent a viable strategy to resolve chemical and biological mesoscale variability in selected areas. Satellite images revealed a number of small structures which were confirmed by in-situ data. Our results document substantial spatial heterogeneity and complexity in surface water carbonate system properties and the magnitude of the CO_2 flux at a horizontal length scale of about 10 km, emphasizing the importance of mesoscale events to regional biogeochemistry. We believe that the resolution of these short length scale distributions provides insight into the biogeochemical dynamics which drive surface and subsurface variability in the Ross Sea. Indeed, predicting future surface Ω_{Ar} and estimating future CO_2 fluxes on a regional scale require understanding of the mesoscale processes controlling the carbonate system.

The distribution of the carbonate system in surface waters was controlled primarily by phytoplankton activity rather than physical forcing, which, on the other hand, created the favorable conditions for the diatoms growth in the upper layer of the water column. The dominance of diatoms versus haptophytes is found to have particular implications for the ratios of nutrient drawdown and carbon (Arrigo et al., 1999).

Acknowledgments

References

Anderson, L.A., Sarmiento, J.L., 1994. Redfield ratios of remineralization determined by nutrient data analysis. Glob. Biogeochem. Cycles 8, 65–80.

Annett, A., Carson, D.S., Crosta, X., Clarke, A., Ganeshram, R.S., 2010. Seasonal progression of diatom assemblages in surface waters of Ryder Bay, Antarctica. Polar Biol. 33, 13–29.

Armand, L.K., Crosta, X., Romero, O., Pichon, J.J., 2005. The biogeography of major diatom taxa in Southern Ocean sediments: 1. Sea ice related species. Palaeogeogr. Palaeoclimatol. Palaeoecol. 223, 93–126. http://dx.doi.org/10.1016/j.palaeo.2005.02.015.

Arrigo, K.R., 2007. Physical control of primary productivity in Arctic and Antarctic polynyas. In: Smith Jr., W.O., Barber, D.G. (Eds.), Polynyas: Windows to the WorldElsevier Oceanography Series 74. Elsevier, Amsterdam, The Netherlands, pp. 223–238.

Arrigo, K.R., van Dijken, G., 2007. Interannual variation in air-sea CO_2 flux in the Ross Sea, Antarctica: a model analysis. J. Geophys. Res. 112, C03020.

Arrigo, K.R., Robinson, D.H., Worthen, D.L., Dunbar, R.B., DiTullio, G.R., VanWoert, M., Lizotte, M.P., 1999. Phytoplankton community structure and the drawdown of nutrients and CO_2 in the Southern Ocean. Science 283, 365–367.

Arrigo, K.R., DiTullio, G.R., Dunbar, R.B., Lizotte, M.P., Robinson, D.H., VanWoert, M., Worthen, D.L., 2000. Phytoplankton taxonomic variability and nutrient utilization and primary production in the Ross Sea. J. Geophys. Res. 105, 8827–8846.

Arrigo, K.R., van Dijken, G., Long, M., 2008. Coastal Southern Ocean: a strong anthropogenic CO_2 sink. Geophys. Res. Lett. 35, L21602. http://dx.doi.org/10.1029/2008.

Bakker, D.C.E., Hoppema, M., Schröder, M., Geibert, W., de Baar, H.J.W., 2008. A rapid transition from ice covered CO_2-rich waters to a biologically mediated CO_2 sink in the eastern Weddell Gyre. Biogeosciences 5, 1373–1386.

Bates, N.R., Hansell, D.A., Carlson, C.A., Gordon, L.I., 1998. Distribution of CO_2 species, estimates of net community production, and air–sea CO_2 exchange in the Ross Sea polynya. J. Geophys. Res. 103, 2883–2896.

Budillon, G., Spezie, G., 2000. Thermohaline structure and variability in the Terra Nova Bay polynya, Ross Sea. Antarct. Sci. 12, 493–508.

Budillon, G., Pacciaroni, M., Cozzi, S., Rivaro, P., Catalano, G., Ianni, C., Cantoni, C., 2003. An optimum multiparameter mixing analysis of the shelf waters in the Ross Sea. Antarct. Sci. 15 (1), 105–118.

Caldeira, K., Duffy, P.B., 2000. The role of the Southern Ocean in uptake and storage of anthropogenic carbon dioxide. Science 287, 620–622.

Caron, D.A., Dennett, M.R., Lonsdale, D.J., Moran, D.M., Shalapyonok, L., 2000. Microzooplankton herbivory in the Ross Sea, Antarctica. Deep-Sea Res. II 47, 3249–3272.

Catalano, G., Budillon, G., La Ferla, R., Povero, P., Ravaioli, M., Saggiomo, V., Accornero, A., Azzaro, M., Carrada, G.C., Giglio, F., Langone, L., Mangoni, O., Misic, C., Modigh, M., 2010. The Ross Sea. In: Liu, K.K., Atkinson, L., Quinones, R., Talaue, McManus L. (Eds.), Carbon and Nutrient Fluxes in Continental Margins: A Global Synthesis. Springer-Verlag, Berlin, Heidelberg, New York, Tokyo, pp. 303–318.

Chen, F., Cai, W.J., Wang, Y., Rii, Y.M., Bidigare, R.R., Benitez-Nelson, C.R., 2008. The carbon dioxide system and net community production within a cyclonic eddy in the lee of Hawaii. Deep-Sea Res. II 55, 1412–1425.

DeJong, H.B., Dunbar, R.B., Mucciarone, D.A., Koweek, D.A., 2015. Carbonate saturation state of surface waters in the Ross Sea and Southern Ocean: controls and implications for the onset of aragonite undersaturation. Biogeosci. Discuss. 12, 8429–8465.

DiTullio, G.R., Grebmeier, J.M., Arrigo, K.R., Lizotte, M.P., Robinson, D.H., Leventer, A., Barry, J., VanWoert, M.L., Dunbar, R.B., 2000. Rapid and early export of *Phaeocystis antarctica* blooms in the Ross Sea, Antarctica. Nature 404, 595–598.

DiTullio, G.R., Geesey, M., Jones, D.R., Daly, K., Campbell, L., Smith Jr., W.O., 2003. Phytoplankton distribution and abundance along 170°W in the South Pacific Ocean. Mar. Ecol. Prog. Ser. 255, 55–80.

DOE (US Department of Energy), 2007. In: Dickson, A.G., Goyet, C. (Eds.), Handbook of Methods for the Analysis of the Various Parameters of the Carbon Dioxide System in Sea Water. Version 3.0.

Dunbar, R.B., Arrigo, K.R., DiTullio, G.D., Leventer, A., Lizotte, M.P., Van Woert, M., Robinson, D.H., 2003. Non Redfield production and export of marine organic matter: a recurrent part of the annual cycle in the Ross Sea, Antarctica. In: Di Tullio, G.R., Dunbar, R.B. (Eds.), Biogeochemistry of the Ross SeaAntarctic Research Series 78. American Geophysical Union, Washington DC, USA, pp. 179–196.

Erofeeva, S.Y., Padman, L., Egbert, G., 2005. Assimilation of ship-mounted ADCP data for barotropic tides: application to the Ross Sea. J. Atmos. Ocean. Technol. 22, 721–734.

Franklin, D.J., Choi, C.J., Hughes, C., Malin, G., Berges, J.A., 2009. Effect of dead phytoplankton cells on the apparent efficiency of photosystem II. Mar. Ecol. Prog. Ser. 382, 35–40.

Garrity, C., Ramseier, R.O., Peinert, R., Kern, S., Fischer, G., 2005. Water column particulate organic carbon modelled fluxes in the ice-frequented Southern Ocean. J. Mar. Syst. 56, 133–149.

Goffart, A., Catalano, G., Hecq, J.H., 2000. Factors controlling the distribution of diatoms and *Phaeocystis* in the Ross Sea. J. Mar. Syst. 27, 161–175.

González-Dávila, M., Santana-Casiano, J.M., Dafner, E.V., 2003. Winter mesoscale variations of carbonate system parameters and estimates of CO_2 fluxes in the Gulf of Cadiz, northeast Atlantic Ocean (February 1998). J. Geophys. Res. 108. http://dx.doi.org/10.1029/2001JC001243.

González-Dávila, M., Santana-Casiano, J.M., de Armas, D., Escánez, J., Suarez-Tangil, M., 2006. The influence of island generated eddies on the carbon dioxide system, south of the Canary Islands. Mar. Chem. 99, 177–190.

Grasshoff, K., 1983. Determination of oxygen. In: Grasshoff, K., Ehrhardt, M., Kremling, K. (Eds.), Methods of Seawater Analysis. WeinheimVerlag Chemie, pp. 61–72.

Haberman, K.L., Ross, R.M., Quetin, L.B., 2003. Diet of the Antarctic krill (*Euphausia superba* Dana): II. Selective grazing in mixed phytoplankton assemblages. J. Exp. Mar. Biol. Ecol. 283, 97–113.

Hales, B., Takahashi, T., 2004. High-resolution biogeochemical investigation of the Ross Sea, Antarctica, during the AESOPS (U. S. JGOFS) Program. Glob. Biogeochem. Cycles 18, GB3006.

Holm-Hansen, O., Lorenzen, C.J., Holmes, R.W., Strickland, J.D.H., 1965. Fluorometric determination of chlorophyll. Journal du Conseil/Conseil Permanent International pour l'Exploration de la Mer 30, 3–15.

Iudicone, D., Rodgers, K.B., Stendardo, I., Aumont, O., Madec, G., Bopp, L., Mangoni, O., Ribera d'Alcala', M., 2011. Water masses as a unifying framework for understanding the Southern Ocean carbon cycle. Biogeosciences 8, 1031–1052.

Kaufman, D.E., Friedrichs, M.A.M., Smith Jr., W.O., Queste, B.Y., Heywood, K.J., 2014. Biogeochemical variability in the southern Ross Sea as observed by a glider deployment. Deep-Sea Res. I 92, 93–106.

Knox, G.A., 1994. The Biology of the Southern Ocean. Cambridge Univ, Press (444 pp.).

Laika, H.E., Goyet, C., Vouve, F., Poisson, A., Touratier, F., 2009. Interannual properties of the CO_2 system in the Southern Ocean south of Australia. Antarct. Sci. 21, 663–680.

Leventer, A., Dunbar, R.B., 1996. Factors influencing the distribution of diatoms and other algae in the Ross Sea. J. Geophys. Res. Oceans 101, 18489–18500.

Mackey, M.D., Mackey, D.J., Higgins, H.W., Wright, S.W., 1996. CHEMTAX—a program for estimating class abundances from chemical markers: application to HPLC measurements of phytoplankton. Mar. Ecol. Prog. Ser. 144, 265–283.

Mangoni, O., Modigh, M., Conversano, F., Carrada, G.C., Saggiomo, V., 2004. Effects of summer ice coverage on phytoplankton assemblages in the Ross Sea, Antarctica. Deep-Sea Res. I 51, 1601–1617.

Mangoni, O., Carrada, G.C., Modigh, M., Catalano, G., Saggiomo, V., 2009a. Photoacclimation in Antarctic bottom ice algae: an experimental approach. Polar Biol. 32, 325–335.

Mangoni, O., Saggiomo, M., Modigh, M., Catalano, G., Zingone, A., Saggiomo, V., 2009b. The role of platelet ice microalgae in seeding phytoplankton blooms in Terra Nova Bay (Ross Sea, Antarctica): a mesocosm experiment. Polar Biol. 32, 311–323.

Manno, C., Sandrini, S., Tositti, L., Accornero, A., 2007. First stages of degradation of *Limacina helicina* shells observed above the aragonite chemical lysocline in Terra Nova Bay (Antarctica). J. Mar. Syst. 68, 91–102.

Massolo, S., Messa, R., Rivaro, P., Leardi, R., 2009. Annual and spatial variations of chemical and physical properties in the Ross Sea surface waters (Antarctica). Cont. Shelf Res. 29, 2333–2344.

Mattsdotter Björk, M., Fransson, A., Torstensson, A., Chierici, M., 2014. Ocean acidification state in western Antarctic surface waters: controls and interannual variability. Biogeosciences 11, 57–73.

McGillicuddy Jr., D.J., Anderson, L.A., Bates, N.R., Bibby, T., Buesseler, K.O., Carlson, C.A., Davis, C.S., Ewart, C., Falkowski, P.G., Goldthwait, S.A., Hansell, D.A., Jenkins, W.J., Johnson, R., Kosnyrev, V.K., Ledwell, J.R., Li, Q.P., Siegel, D.A., Steinberg, D.K., 2007. Eddy/wind interactions stimulate extraordinary mid-ocean plankton blooms. Science 316, 1021–1026.

McNeil, B.I., Tagliabue, A., Sweeney, C., 2010. A multi-decadal delay in the onset of corrosive 'acidified' waters in the Ross Sea of Antarctica due to strong air–sea CO_2 disequilibrium. Geophys. Res. Lett. 37, L19607.

Millero, F., 2007. The marine inorganic carbon cycle. Chem. Rev. 107, 308–341.

Mitchell, B.G., Holm-Hansen, O., 1991. Observation and modeling of the Antarctic phytoplankton crop in relation to mixing depth. Deep-Sea Res. 38, 981–1007.

Moore, J.K., Abbott, M.R., 2000. Phytoplankton chlorophyll distributions and primary production in the Southern Ocean. J. Geophys. Res. 105 (28,709-28,722).

Omand, M.M., D'Asaro, E.A., Lee, C.M., Perry, M.J., Briggs, N., Cetinić, I., Mahadevan, A., 2015. Eddy-driven subduction exports particulate organic carbon from the spring bloom. Science 348, 222–225.

Ori, C., Lenaz, R., Colombo, T., Giovanelli, G., 1996. Atmospheric CO_2 concentration measured continuously from the Mediterranean to the Bellingshausen Sea: technology and methodology. Proceedings 6th Workshop Italian Research on Antarctic Atmosphere, Firenze, 1995. SIF, Bologna, pp. 361–367.

Orsi, A.H., Wiederwohl, C.L., 2009. A recount of Ross Sea waters. Deep-Sea Res. II 56, 778–795.

Peloquin, J.A., Smith Jr., W.O., 2007. Phytoplankton blooms in the Ross Sea, Antarctica: interannual variability in magnitude, temporal patterns, and composition. J. Geophys. Res. 112, C08013. http://dx.doi.org/10.1029/2006JC003816.

Petrou, K., Hassler, C.S., Doblin, M.A., Shelly, K., Schoemann, V., van den Enden, R., Wright, S., Ralph, P.J., 2011. Iron-limitation and high light stress on phytoplankton populations from the Australian Sub-Antarctic Zone (SAZ). Deep-Sea Res. II 58, 2200–2211.

Pierrot, D., Lewis, E., Wallace, D.W.R., 2006. MS Excel Program developed for CO_2 system calculations, ORNL/CDIAC-105. Oak Ridge, TN: Carbon Dioxide Information Analysis Center, Oak Ridge National Laboratory, US Department of Energy.

Reddy, T.E., Arrigo, K.R., 2006. Constraints on the extent of the Ross Sea phytoplankton bloom. J. Geophys. Res. 111, C07005. http://dx.doi.org/10.1029/2005JC003339.

Rivaro, P., Messa, R., Massolo, S., Frache, R., 2010. Distributions of carbonate properties along the water column in the Mediterranean Sea: spatial and temporal variations. Mar. Chem. 121, 236–245.

Rivaro, P., Abelmoschi, M.L., Grotti, M., Magi, E., Margiotta, F., Massolo, S., Saggiomo, V., 2012. Combined effects of hydrographic structure and iron and copper availability on the phytoplankton growth in Terra Nova Bay Polynya (Ross Sea, Antarctica). Deep-Sea Res. I 62, 97–110.

Rivaro, P., Messa, R., Ianni, C., Magi, E., Budillon, G., 2014. Distribution of total alkalinity and pH in the Ross Sea (Antarctica) waters during austral summer 2008. Polar Res. 33, 20403 (http://dx.doi.org/10.3402/polar.v33.20403).

Robertson, J.E.C., Robinson, D.R., Turner, P.M., Holligan, A.J., Watson, P., Boyd, E., Fernandez Finch, M., 1994. The impact of a coccolithophore bloom on oceanic carbon uptake in the northeast Atlantic during summer 1991. Deep-Sea Res. I 41, 297–314.

Russo, A.D.P.G., de Souza, M.S., Mendes, C.F.B., Jesus, B., Tavano, V.M., Garcia, C.A.E., 2015. Photophysiological effects of Fe concentration gradients on diatom-dominated phytoplankton assemblages in the Antarctic Peninsula region. J. Exp. Mar. Biol. Ecol. 466, 49–58.

Sabine, C.L., Feely, R.A., Gruber, N., Key, R.M., Lee, K., Bullister, J.L., Wanninkhof, R., Wong, C.S., Wallace, D.W.R., Tilbrook, B., Millero, F.J., Peng, T., Kozyr, A., Ono, T., Rios, A.F., 2004. The oceanic sink for anthropogenic CO_2. Science 305, 367–371.

Saggiomo, V., Carrada, G.C., Mangoni, O., Ribera d'Alcalà, M., Russo, A., 1998. Spatial and temporal variability of size fractionated biomass and primary production in the Ross Sea (Antarctica) during the austral spring and summer. J. Mar. Syst. 17, 115–127.

Saggiomo, V., Carrada, G.C., Mangoni, O., Marino, D., Ribera d'Alcala`, M., 2000. Physiological and ecological aspects of primary production in the Ross Sea. In: Faranda, F.M., Guglielmo, L., Ianora, A. (Eds.), Ross Sea Ecology—Italian Antarctic Expeditions (1987–1995). Springer, Berlin, pp. 247–258.

Saggiomo, V., Catalano, G., Mangoni, O., Budillon, G., Carrada, G.C., 2002. Primary production processes in ice-free waters of the Ross Sea (Antarctica) during the austral summer 1996. Deep-Sea Res. II 49, 1787–1801.

Sandrini, S., Aït-Ameur, N., Rivaro, P., Massolo, S., Touratier, F., Tositti, L., Goyet, C., 2007. Anthropogenic carbon distribution in the Ross Sea (Antarctica). Antarct. Sci. 19, 395–407.

Schlitzer, R., Ocean Data View, odv.awi.de, 2015.

Schoemann, V., Becquevort, S., Stefels, J., Rousseau, V., Lancelot, C., 2005. *Phaeocystis* blooms in the global ocean and their controlling mechanisms: a review. J. Sea Res. 53, 43–66.

Schreiber, U., Bilger, W., Neubauer, C., 1994. Chlorophyll fluorescence as a non-intrusive indicator for rapid assessment of *in vivo* photosynthesis. Ecol. Stud. 100, 49–70.

Schreiber, U., Hormann, H., Neubauer, C., Klughammer, C., 1995. Assessment of photosystem II photochemical quantum yield by chlorophyll fluorescence quenching analysis. Aust. J. Plant Physiol. 22, 209–220.

Smith Jr., W.O., Asper, V.L., 2001. The influence of phytoplankton assemblage composition on biogeochemical characteristics and cycles in the southern Ross Sea, Antarctica. Deep-Sea Res. I 48, 137–161.

Smith Jr., W.O., Comiso, J.C., 2008. Influence of sea ice on primary production in the Southern Ocean: a satellite perspective. J. Geophys. Res. 113, C05S93. http://dx.doi.org/10.1029/2007JC004251.

Smith Jr., W.O., Gordon, L.I., 1997. Hyperproductivity of the Ross Sea (Antarctica) polynya during austral spring. Geophys. Res. Lett. 24, 233–236.

Smith Jr., W.O., Dinniman, M.S., Tozzi, S., DiTullio, G.R., Mangoni, O., Modigh, M., Saggiomo, V., 2010. Phytoplankton photosynthetic pigments in the Ross Sea: patterns and relationships among functional groups. J. Mar. Syst. 82, 177–185.

Smith Jr., W.O., Shields, A.R., Dreyer, J., Peloquin, J.A., Asper, V., 2011a. Interannual variability in vertical export in the Ross Sea: magnitude, composition, and environmental correlates. Deep- Sea Res. I 58, 147–159.

Smith Jr., W.O., Asper, V., Tozzi, S., Liu, X., Stammerjohn, S.E., 2011b. Surface layer variability in the Ross Sea, Antarctica as assessed by in situ fluorescence measurements. Prog. Oceanogr. 88, 28–45.

Smith Jr., W.O., Tozzi, S., Sedwick, P.W., DiTullio, G.R., Peloquin, J.A., Long, M., Dunbar, R., Hutchins, D.A., Kolber, Z., 2013. Spatial and temporal variations in variable fluorescence in the Ross Sea (Antarctica): environmental and biological correlates. Deep-Sea Res. I 79, 141–155.

Smith Jr., W.O., Ainley, D.G., Arrigo, K.R., Dinniman, M.S., 2014. The oceanography and ecology of the Ross Sea. Ann. Rev. Mar. Sci. 6, 469–487.

Sullivan, C.W., Arrigo, K.R., McClain, C.R., Comiso, J.C., Firestone, J., 1993. Distributions of phytoplankton blooms in the Southern Ocean. Science 262, 1832–1837.

Sweeney, C., 2003. The annual cycle of surface CO_2 and O_2 in the Ross Sea: a model for gas exchange on the continental shelves of Antarctica. In: DiTullio, G.R., Dunbar, R.B. (Eds.), Biogeochemistry of the Ross Sea. Antarctic Research Series 78. American Geophysical Union, Washington, DC, USA, pp. 295–312.

Sweeney, C., Hansell, D.A., Carlson, C.A., Codispoti, L.A., Gordon, L.I., Marra, J., Millero, F.J., Smith Jr., W.O., Takahashi, T., 2000. Biogeochemical regimes, net community production and carbon export in the Ross Sea, Antarctica. Deep-Sea Res. II 47, 3369–3394.

Sweeney, E.N., McGillicuddy Jr., D.J., Buesseler, K.O., 2003. Biogeochemical impacts due to mesoscale eddy activity in the Sargasso Sea as measured at the Bermuda Atlantic Time-Series Study (BATS). Deep-Sea Res. II 50, 3017–3039.

Tortell, P.D., Guéguen, C., Long, M.C., Payne, C.D., Leeand, P., Di Tullio, G.R., 2011. Spatial variability and temporal dynamics of surface water pCO2, ΔO2/Ar and dimethylsulfide in the Ross Sea, Antarctica. Deep-Sea Res. I 58, 241–259.

Tréguer, P., Nelson, D.M., Van Bennekom, A.J., DeMaster, D.J., Leynaert, A., Quéguiner, B., 1995. The silica balance in the world ocean: a re estimate. Science 268, 375–379.

Tremblay, J.E., Smith Jr., W.O., 2007. Primary production and nutrient dynamics in polynyas. In: Smith Jr., W.O., Barber, D.G. (Eds.), Polynyas: Windows to the WorldElsevier Oceanography Series 74. Elsevier, Amsterdam, The Netherlands, pp. 239–269.

Utermöhl, H., 1958. Zur vervollkommnung der quantitativen phytoplankton-methodik. Mitt. Int. Ver. Theor. Angew. Limnol. 9, 1–38 (Villac.).

van Boekel, W.H.M., Hansen, F.C., Riegman, R., Bak, R.P.M., 1992. Lysis-induced decline of a *Phaeocystis* spring bloom and coupling with the microbial food web. Mar. Ecol. Prog. Ser. 81, 269–276.

van de Poll, W.H., van Leeuwe, M.A., Roggeveld, J., Buma, A.G.J., 2005. Nutrient limitation and high irradiance acclimation reduce par and UV-induced viability loss in the Antarctic diatom *Chaetoceros brevis* (Bacillariophyceae). J. Phys. 41, 840–850.

Veldhuis, M.J.W., Kraay, G.W., Timmermans, K.R., 2001. Cell death in phytoplankton: correlation between changes in membrane permeability, photosynthetic activity, pigmentation and growth. Eur. J. Phycol. 36, 167–177.

Verity, P.G., Smetacek, V., 1996. Organism life cycles, predation, and the structure of marine pelagic ecosystems. Mar. Ecol. Prog. Ser. 130, 277–293.

Vidussi, F., Claustre, H., Bustillos-Guzm_an, J., Cailliau, C., Marty, J.C., 1996. Determination of chlorophylls and carotenoids of marine phytoplankton: separation of chlorophyll a from divinylchlorophyll a and zeaxanthin fromlutein. J. Plankton Res. 18 (12), 2377–2382.

Wanninkhof, R., 1992. Relationship between wind speed and gas exchange over the ocean. J. Geophys. Res. 97, 7373–7382.